AD-A040 421 CALIFORNIA INST OF TECH PASADENA DIV OF CHEMISTRY A--ETC F/G 20/8
DOUBLE RESONANCE INTERFEROMETRY: RELAXATION TIMES FOR DIPOLAR F--ETC(U)
APR 77 M E STOLL, A J VEGA, R W VAUGHAN N00014-75-C-0960

UNCLASSIFIED TR-6 NL

| OF |
AD
A040421

END

DATE
FILMED
7-77

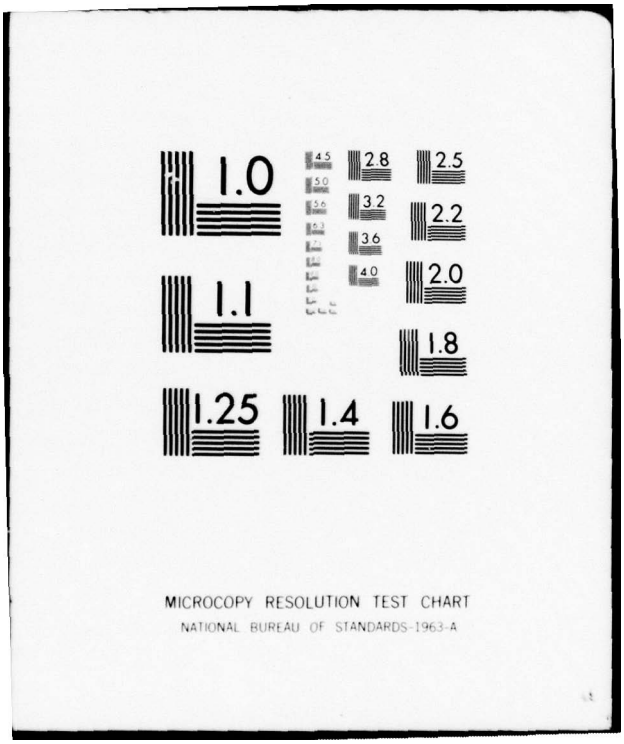
1.0
4.5
5.0
5.6
2.8
3.2
3.6
4.0
2.5
2.2
2.0
1.8
1.1
1.25
1.4
1.6
MICROCOPY RESOLUTION TEST CHART
NATIONAL BUREAU OF STANDARDS-1963-A

Unclassified
SECURITY CLASSIFICATION OF THIS PAGE (When Data Entered)

AD A040421

REPORT DOCUMENTATION PAGE

READ INSTRUCTIONS BEFORE COMPLETING FORM

1. REPORT NUMBER: Technical Report #6
2. GOVT ACCESSION NO.: (9) Interim rept.
3. RECIPIENT'S CATALOG NUMBER: (12)

4. TITLE (and Subtitle): (6) DOUBLE RESONANCE INTERFEROMETRY: RELAXATION TIMES FOR DIPOLAR FORBIDDEN TRANSITIONS AND OFF-RESONANCE EFFECTS IN AN AX SPIN SYSTEM.
5. TYPE OF REPORT & PERIOD COVERED: interim, Technical Report #6
6. PERFORMING ORG. REPORT NUMBER:

7. AUTHOR(s): (10) M. E. Stoll, A. J. Vega, and R. W. Vaughan
8. CONTRACT OR GRANT NUMBER(s): (15) N00014-75-C-0960; NSG-7275

9. PERFORMING ORGANIZATION NAME AND ADDRESS:
Division of Chemistry & Chemical Engineering
California Institute of Technology
Pasadena, California 91125

10. PROGRAM ELEMENT, PROJECT, TASK AREA & WORK UNIT NUMBERS: NR-056-605

11. CONTROLLING OFFICE NAME AND ADDRESS:
ONR Branch Office ATTN: Dr. R. J. Marcus
1030 East Green Street
Pasadena, California 91106

12. REPORT DATE: 4/77 (12) 47 p.
13. NUMBER OF PAGES: 40

14. MONITORING AGENCY NAME & ADDRESS (if different from Controlling Office): (14) TR-6 (11) apr 77

15. SECURITY CLASS. (of this report): Unclassified
15a. DECLASSIFICATION/DOWNGRADING SCHEDULE:

16. DISTRIBUTION STATEMENT (of this Report)

Approved for public release; distribution unlimited

DDC RECEIVED JUN 9 1977 D

17. DISTRIBUTION STATEMENT (of the abstract entered in Block 20, if different from Report)

18. SUPPLEMENTARY NOTES

Submitted for publication

19. KEY WORDS (Continue on reverse side if necessary and identify by block number)

NMR interferometry, double resonance, nuclear magnetic resonance, spin dynamics, spinor character

20. ABSTRACT (Continue on reverse side if necessary and identify by block number)

Experimental and theoretical results of a nuclear magnetic double resonance interferometric study of a model AX spin system are presented. Measurements of the characteristic relaxation times of off-diagonal density matrix elements corresponding to magnetic-dipole-forbidden transitions are presented, and the use of such relaxation time constants to obtain information including cross-correlations of the fluctuating fields at the A and X nuclear sites is discussed.

DD FORM 1 JAN 73 1473 EDITION OF 1 NOV 65 IS OBSOLETE
S/N 0102 LF 014 6601

Unclassified
SECURITY CLASSIFICATION OF THIS PAGE (When Data Entered)

AD No. ____
DDC FILE COPY

071575

Double Resonance Interferometry: Relaxation Times for Dipolar Forbidden Transitions and Off-Resonance Effects in an AX Spin System

M. E. Stoll, A. J. Vega[+], and R. W. Vaughan

Division of Chemistry and Chemical Engineering
California Institute of Technology
Pasadena, California 91125

ABSTRACT

Experimental and theoretical results of a nuclear magnetic double resonance interferometric study of a model AX spin system are presented. Measurements of the characteristic relaxation times of off-diagonal density matrix elements corresonding to magnetic-dipole-forbidden transitions are presented, and the use of such relaxation time constants to obtain information including cross-correlations of the fluctuating fields at the A and X nuclear sites is discussed. Off-resonance effects produce large changes in the spectra, and exploitation of these effects to indirectly measure the precise resonance frequency of a spin with a small magnetogyric ratio is discussed.

I. INTRODUCTION

This paper presents a detailed analysis of the application of a recently presented interferometric spectroscopic technique[1] to a model AX spin system. The density matrix for such a coupled spin ½ system is a four-by-four matrix, and when such a spin system in a strong magnetic field is prepared in a nonequilibrium state, the subsequent relaxation of the system to thermal equilibrium can be described by the decay of the elements of the density matrix, where the diagonal elements relax with characteristic time constants, called T_1's, and the off-diagonal elements relax with characteristic time constants called T_2's[2,3]. The determination of all of the T_1's requires a sequence of experiments, and this has been discussed recently in detail for an AX system by Mayne, Adlerman, and Grant[4], while measurement of the off-diagonal relaxation rates corresponding to magnetic-dipole-allowed transitions involves application of a standard Carr-Purcell sequence. This leaves off-diagonal rates corresponding to magnetic-dipole-forbidden transitions to be measured, and the present paper presents a simple method for direct measurement of these remaining relaxation rates. These rates are of particular interest since they can contain cross-correlation information about the fluctuating fields at the sites of the coupled A and X nuclei. In our review of the literature we have found no reports of previous efforts to measure these relaxation rates in coupled spin ½ systems, although we do want to call attention to an effort to detect such dipolar-forbidden transitions by a multiple step excitation process, and that effort involved a spin 5/2 nucleus, ^{27}Al in Al_2O_3[5].

In addition, the analysis of off-resonance phase effects measured in the spectra demonstrate that one can use such an interferometric scheme to measure indirectly the resonance frequency of one of the coupled nuclei by observation of

the spectra of only the second nucleus. The limiting precision of such an indirect measurement will be shown to be equivalent to that of a direct measurement. This could be of use when the magnetogyric ratios of the two coupled spins differ by a large amount, and the direct observation of the nucleus with the smaller magnetogyric ratio is made difficult by poor signal-to-noise conditions.

II. DESCRIPTION AND EXPLANATION OF THE EXPERIMENT

A. General Description

The system we chose for this experiment was a conventional AX(^{13}C - ^{1}H) system where both nuclei are spin ½. The ^{13}C (S spin) and ^{1}H (I spin) were in a liquid and were weakly coupled to each other via a scalar coupling of the form $J \underset{\sim}{I} \cdot \underset{\sim}{S}$. Since the sample was in a strong magnetic field, oriented along the z-axis, only the secular part of the scalar interaction, $J I_z S_z$, contributed to first order to the energy level spacings for this system. An appropriate energy-level diagram is shown in Figure 1. The four levels are the eigenstates of the Zeeman Hamiltonian corresponding to $\alpha\alpha$, $\alpha\beta$, $\beta\alpha$, and $\beta\beta$, where the α and β represent the spin "up" and "down" states with the z-component of angular momentum equal to $\frac{1}{2}\hbar$ and $-\frac{1}{2}\hbar$, and the first Greek letter refers to the I spin while the second refers to the S spin. Note that the secular part of the scalar interaction alters the energy levels slightly (exaggerated considerably in Figure 1 for purposes of explanation), thus giving rise to four inequivalent magnetic-dipole-allowed transitions. The ^{1}H NMR spectrum is a doublet corresonding to transitions 1-3 and 2-4 (single arrows), and the ^{13}C spectrum is also a doublet corresponding to transitions 1-2and 3-4 (double arrows). This doublet splitting is crucial for the present experiment since it enables us to selectively irradiate certain transitions.

The experiment is shown schematically in Figure 2. First, we apply a nonselective $\pi/2$ pulse (2 μsec) to both the proton transitions. Then immediately after the $\pi/2$ pulse we apply a low-power, selective pulse of length τ to only one of the ^{13}C transitions. At a time ΔT after the original proton $\pi/2$ pulse we apply another nonselective π pulse (4 μsec) to both proton transitions, causing a proton spin echo to be formed at time $2\Delta T$. The decay taken from time t = 0

(at the middle of the echo) is recorded for Fourier transformation (FT). The five spectra shown in Figure 3 are such FT spectra for values of τ = 0, 28, 56, 84, and 112 msec. The top spectrum, for which τ = 0, corresponds to a conventional spin echo pulsed NMR-FT proton spectrum. The sample was a solution of 91% ^{13}C-enriched sodium formate ($NaCHO_2$) dissolved in D_2O with a small amount of ^1H impurity. It is the ^1H and the ^{13}C in the enriched formate ions that comprise our AX spin system and give rise to the symmetric proton doublet split by J = 195 Hz. The small peak at the center of the doublet is due to the protons in the 9% of the formate ions containing spinless ^{12}C. The large peak on the far left is due to the small amount of proton impurity in the D_2O. When preparing the solution, no efforts were made to remove dissolved oxygen.

When looking at the spectra of Figure 3, two effects stand out. First, we see that the amplitude of the formate doublet actually goes to zero, then negative, back to zero, and finally positive again. Secondly, the amplitudes of both members of the doublet do not remain the same. The former effect can be explained completely by the spin dynamics of the system[1] while the latter effect can be explained only by invoking relaxation phenomena. Therefore, in order to understand the results of this experiment, we must theoretically understand the spin dynamics of such a system first without, and later with, relaxation effects taken into account.

B. Spin Dynamics Ignoring Off-Resonance and Relaxation Effects

We first examine the spin dynamics of our experiment, ignoring relaxation effects as well as effects of the ^{13}C selective pulse being "off-resonance." There are, in fact, two such off-resonance effects to be ignored. The first is the possibility of the selective r.f. radiation being at a slightly different frequency from the ^{13}C transition frequency. The second is the possibility

that although the selective radiation is weak, it still is strong enough to somewhat disturb the other ^{13}C transition.

Before we apply the first pulse, we assume that our spin system is in thermal equilibrium and that it can be described by the following 4 x 4 density matrix:

$$\rho_{equil} \doteq \begin{bmatrix} A & 0 & 0 & 0 \\ 0 & B & 0 & 0 \\ 0 & 0 & C & 0 \\ 0 & 0 & 0 & D \end{bmatrix} \qquad (1)$$

where the basis states are chosen to be the states 1, 2, 3, and 4 of Figure 1 ($\alpha\alpha$, $\alpha\beta$, $\beta\alpha$, and $\beta\beta$, respectively). Note that the off-diagonal matrix elements are zero, meaning there is no statistical phase coherence in the system and, furthermore, in the high temperature approximation

$$A - B = C - D \qquad (2)$$

As usual, the observable ^{1}H and ^{13}C magnetizations are proportional to the expectation values of the dimensionless spin operators, I and S. The expectation values for I and S corresponding to the various observable magnetizations are related to the density matrix elements as follows:

$$\begin{aligned} \langle I_x \rangle_{13} &= \text{Re } \rho_{13} \quad , & \langle I_x \rangle_{24} &= \text{Re } \rho_{24} \\ \langle I_y \rangle_{13} &= -\text{Im } \rho_{13} \quad , & \langle I_y \rangle_{24} &= -\text{Im } \rho_{24} \\ \langle I_z \rangle_{13} &= \tfrac{1}{2}(\rho_{11} - \rho_{33}) \quad , & \langle I_z \rangle_{24} &= \tfrac{1}{2}(\rho_{22} - \rho_{44}) \\ \langle S_x \rangle_{12} &= \text{Re } \rho_{12} \quad , & \langle S_x \rangle_{34} &= \text{Re } \rho_{34} \end{aligned} \qquad (3)$$

$$\langle S_y \rangle_{12} = -\mathrm{Im}\,\rho_{12} \quad , \quad \langle S_y \rangle_{34} = -\mathrm{Im}\,\rho_{34}$$

$$\langle S_z \rangle_{12} = \tfrac{1}{2}(\rho_{11} - \rho_{22}) \quad , \quad \langle S_z \rangle_{34} = \tfrac{1}{2}(\rho_{33} - \rho_{44})$$

Because of the hermiticity of the density matrix, $\mathrm{Re}\rho_{ij} = \mathrm{Re}\rho_{ji}$ and $\mathrm{Im}\rho_{ij} = -\mathrm{Im}\rho_{ji}$. The subscripts refer to particular levels between which transitions give rise to observable magnetization. Because of the scalar splitting, we can distinguish between the transverse magnetization $\langle I_x \rangle_{13}$ and $\langle I_x \rangle_{24}$, etc. Each corresponds to one of the peaks of the doublet. However, since we do not know the sign of J, we do not know which magnetization corresponds to which peak. Fortunately, this is no serious drawback, and we will say more about this point later in the paper.

Initially, since the off-diagonal elements are zero, there is no transverse magnetization. The purpose of the proton $\pi/2$ is then to create some transverse magnetization and phase coherence. After the $\pi/2$ pulse, (assumed to be along the x-axis of the proton rotating frame), we have the following matrix, making use of Equation (2) and ignoring effects due to the finite width of the pulse:

$$\rho(0) = \begin{bmatrix} \frac{1}{2}(A+C) & 0 & \frac{1}{2}i(A-C) & 0 \\ 0 & \frac{1}{2}(B+D) & 0 & \frac{1}{2}i(A-C) \\ -\frac{1}{2}i(A-C) & 0 & \frac{1}{2}(A+C) & 0 \\ 0 & -\frac{1}{2}i(A-C) & 0 & \frac{1}{2}(B+D) \end{bmatrix} \qquad (4)$$

The Hamiltonian acting on the system during the weak ^{13}C pulse is (for $\hbar = 1$):

$$H = \omega_I I_z + \omega_S S_z + J I_z S_z + 2\omega_1 S_x \cos \omega t \tag{5}$$

where we have chosen the pulse to be along the x-axis of the ^{13}C rotating frame. The frequencies ω_I and ω_S are the Larmor frequencies of the ^1H and ^{13}C, ω is the frequency of the ^{13}C pulse, $2\omega_1$ is its amplitude, and J is the scalar coupling in radians per second. We now analyze this by transforming to a doubly rotating frame in which the Hamiltonian is static, by choosing to go to the interaction frame of:

$$H_o = \omega S_z + \omega_p I_z \tag{6}$$

where ω_p is the reference frequency of the phase detector we used to detect the proton traverse magnetization. After transforming to this frame we have the following Hamiltonian

$$H' = \Delta\omega I_z + \tfrac{1}{2} J \ S_z + J I_z S_z + \omega_1 S_x$$

$$\Delta\omega = \omega_I - \omega_p \tag{7}$$

$$\omega_S - \omega = \tfrac{1}{2} J$$

ignoring the counter-rotating r.f. component as usual. The density matrix ρ is also taken to be in this same rotating frame, and for the sake of simplicity we will not use any special notation to indicate this. Equation (4) is still correct because we have assumed the lab frame and the interaction frame to be coincident before the $\pi/2$ pulse, and we are justifiably assuming the pulse is short enough to ignore effects during the pulse. The density matrix evolves in time according to the Liouville equation:

$$\frac{d}{dt}\rho = i\,[\rho, H'] \tag{8}$$

Using Equations (7) we have the following matrix for H':

$$H' = \begin{bmatrix} \frac{1}{2}(J+\Delta\omega) & \frac{1}{2}\omega_1 & 0 & 0 \\ \frac{1}{2}\omega_1 & -\frac{1}{2}(J-\Delta\omega) & 0 & 0 \\ 0 & 0 & -\frac{1}{2}\Delta\omega & \frac{1}{2}\omega_1 \\ 0 & 0 & \frac{1}{2}\omega_1 & -\frac{1}{2}\Delta\omega \end{bmatrix} \tag{9}$$

The first kind of previously mentioned off-resonance effect was ignored when we chose $\omega - \omega_S = \frac{1}{2} J$, from Equations (7), because the ^{13}C radiation is being applied right "on" one of the resonances of the doublet. The second kind of off-resonance effect is ignored by assuming that

$$J >> \tfrac{1}{2}\omega_1 \text{ or } |H'_{11} - H'_{22}| >> H'_{12} \tag{10}$$

This approximation means that the r.f. perturbation is so weak that it does not mix levels 1 and 2, thus we set $H'_{12} = H'_{21} = 0$. However, levels 3 and 4 are still very strongly mixed by the ^{13}C pulse.

Because this experiment involves observing only the I transverse magnetization, Equations (3) show that it is sufficient to calculate only ρ_{13} and ρ_{24} (or ρ_{31} and ρ_{42}), and thus we shall only worry about determining these matrix elements. Using Equations (8) and (9) we can write the following differential equations, and their initial conditions using Equation (4):

$$
\begin{aligned}
\dot{\rho}_{13} &= -i\,(\tfrac{1}{2}J + \Delta\omega)\,\rho_{13} + i\,\tfrac{1}{2}\omega_1\,\rho_{14} \\
\dot{\rho}_{14} &= -i\,(\tfrac{1}{2}J + \Delta\omega)\,\rho_{14} + i\,\tfrac{1}{2}\,\omega_1\,\rho_{13} \\
\dot{\rho}_{24} &= \;\;i\,(\tfrac{1}{2}J - \Delta\omega)\,\rho_{24} + i\,\tfrac{1}{2}\,\omega_1\,\rho_{23} \\
\dot{\rho}_{23} &= \;\;i\,(\tfrac{1}{2}J - \Delta\omega)\,\rho_{23} + i\,\tfrac{1}{2}\,\omega_1\,\rho_{24}
\end{aligned}
\tag{11}
$$

$$\rho_{13}\,(0) = \rho_{24}\,(0) = \tfrac{1}{2}\,i\,(A - C)$$

$$\rho_{14}\,(0) = \rho_{23}\,(0) = 0$$

Solving these equations, we can determine the relevant matrix elements at the end of the ^{13}C pulse of length τ

$$
\begin{aligned}
\rho_{13}\,(\tau) &= \tfrac{1}{2}\,i\,(A - C)\,e^{-i(\frac{1}{2}J + \Delta\omega)\tau}\cos(\tfrac{1}{2}\,\omega_1\tau) \\
\rho_{24}\,(\tau) &= \tfrac{1}{2}\,i\,(A - C)\,e^{\;\;i(\frac{1}{2}J - \Delta\omega)\tau}\cos(\tfrac{1}{2}\,\omega_1\tau)
\end{aligned}
\tag{12}
$$

The time evolution of the density matrix from the time τ through the π proton pulse at ΔT, which we take to be along the x-axis of the proton rotating frame, and finally up to the middle of the echo at $2\Delta T$, is quite straightforward to calculate, and we merely state the pertinent results:

$$
\begin{aligned}
\rho_{31}\,(2\Delta T) &= e^{\;\;i(\frac{1}{2}J + \Delta\omega)\tau}\,\rho_{13}\,(\tau) \\
\rho_{42}\,(2\Delta T) &= e^{-i(\frac{1}{2}J - \Delta\omega)\tau}\,\rho_{24}\,(\tau)
\end{aligned}
\tag{13}
$$

Thus, from Equations (12) and (13), we have

$$\rho_{31}\,(2\Delta T) = \tfrac{1}{2}\, i\,(A - C)\cos\,(\tfrac{1}{2}\omega_1\tau)$$
$$\rho_{42}\,(2\Delta T) = \tfrac{1}{2}\, i\,(A - C)\cos\,(\tfrac{1}{2}\omega_1\tau) \qquad (14)$$

We can then use Equations (3) to compute the transverse proton magnetization of the two peaks in the ^1H doublet

$$\langle I_y\,(2\Delta T)\rangle_{13} = \langle I_y\,(2\Delta T)\rangle_{24} = \langle I_y\,(2\Delta T)\rangle_{\tau=0}\ \cos\,(\tfrac{1}{2}\omega_1\tau)$$
$$\langle I_x\,(2\Delta T)\rangle_{13} = \langle I_x\,(2\Delta T)\rangle_{24} = 0 \qquad (15)$$

where $\langle I_y(2\Delta T)\rangle_{\tau=0}$ is just the magnitude of the transverse magnetization at $2\Delta T$ (the middle of the echo) for the case in which $\tau = 0$ (no ^{13}C irradiation). Thus, we see that the effect of our selective ^{13}C pulse is to cause the proton magnetization to oscillate sinusoidally with a frequency of $\frac{1}{2}\omega_1$. So by choosing the length of τ to correspond to a normal 2π pulse ($\omega_1\tau = 2\pi$) we see that effect is to multiply the amplitude of the proton doublet by $\cos(\pi) = -1$. This effect is the manifestation of the spinor character of the pseudo-two-level system composed of levels 3 and 4, and this phenomenon has been discussed in detail elsewhere[1]. The spectra in Figure 3 were taken for values of τ corresponding to values of $\omega_1\tau = 0, \pi, 2\pi, 3\pi$, and 4π. Note that after a full 4π rotation the phase of the proton magnetization has come back to itself again, which is further consistent with spinor behavior. Thus, we can see that this idealized spin dynamical approach can at least explain the oscillatory behavior in Figure 3. However, we need to understand quantitatively the amplitudes of both members of the doublet, and this can only be done by appealing to relaxation effects.

By examining Equations (15), one notes that the magnetization linearly oscillates rather than precesses. By looking at Equations (11) we see that the matrix elements ρ_{13} and ρ_{14} are coupled, as well as ρ_{24} and ρ_{23}. Solving for ρ_{14} would show that $\rho_{14} \propto \sin(\frac{1}{2}\omega_1\tau)$; therefore, we see that ρ_{13} and ρ_{14} are mutually oscillating and when one has a maximum, the other is zero, and vice versa. According to the definition of the density matrix:

$$\rho_{ij} = \overline{C_i C_j^*} \tag{16}$$

where C_i and C_j are the complex quantum mechanical amplitudes for the system to be in the states i and j, and the bar represents the mixed state which results from taking a statistical ensemble average over the system. Thus, we see that when $\rho_{14} \neq 0$, statistically our system is in a linear combination of states 1 and 4. This, in turn, means that there is phase coherence or "magnetization" corresponding to the forbidden transition 1-4. The reason we do not see this magnetization is twofold. First of all, since it is magnetic-dipole-forbidden, the process is second order and the probability of the transition is correspondingly low. Secondly, the 1-4 transition frequency is at about $\omega_I + \omega_S$, and we would have to make our phase detection reference frequency ω_p closer to this "double quantum" frequency in order to observe this magnetization. Similarly, ρ_{24} and ρ_{23} form a complementary pair of oscillating variables, and $\rho_{23} \neq 0$ implies phase coherence between the levels 2 and 3, which corresponds to a magnetic-dipole-forbidden "flip-flop" transition. In anticipation of our later discussion of relaxation effects, we mention that if the off-diagonal element ρ_{14} relaxes with a different rate than ρ_{13}, we would expect the amplitude of the 1-3 peak of the doublet to be different from the prediction of Equation (15). This is because for $\tau \neq 0$, the system has a probability of being in a linear combination of states 1 and 4 as well

as 1 and 3. Thus, the ratio of $\langle I_y(2\Delta T)\rangle$ to $\langle I_y(2\Delta T)\rangle_{\tau=0}$ could be either smaller or larger than that predicted by Equation (15), depending on whether or not the relaxation rate of ρ_{14} is faster or slower than the relaxation rate of ρ_{13}. Again, similar statements can be made about the rates of ρ_{24} and ρ_{23}. Thus, by attempting to quantitatively fit the amplitudes of the peaks of the formate doublet for different values of τ, we can in fact determine the relaxation rates of the density matrix elements ρ_{14} and ρ_{23}. In the next section we pursue the effects of being "off-resonance" on the ^{13}C frequency, while still ignoring relaxation. We will see that these "off-resonance" effects cannot explain the fact that the doublet does not remain symmetric.

C. Spin Dynamics Including Off-Resonance Effects but Ignoring Relaxation Effects

As mentioned earlier, there are two important "off-resonance" effects of the selective ^{13}C pulse to be considered. These both fall naturally out of the mathematics, if we choose the proper interaction frame. We start with the same Hamiltonians as those in Equations (5) and (6); however, we will choose our frequency of ^{13}C irradiation, ω, slightly differently. In this case Equations (7) must be modified so that now after transformation to the interaction frame, we have the following remaining Hamiltonian:

$$H' = \Delta\omega\, I_z + (\tfrac{1}{2}J + \delta\omega)\, S_z + J\, I_z\, S_z + \omega_1\, S_x$$

$$\Delta\omega = \omega_I - \omega_p \qquad (17)$$

$$\omega_S - \omega = \tfrac{1}{2}J + \delta\omega$$

Therefore $\delta\omega$ is just the difference in frequency between the applied ^{13}C radiation frequency and the frequency of the one member of the doublet we are

intending to irradiate, and thus $\delta\omega$ measures an "off-resonance" effect. Using Equations (17) we can now write the matrix representing H'

$$H' = \begin{bmatrix} \frac{1}{2}(J+\delta\omega+\Delta\omega) & \frac{1}{2}\omega_1 & 0 & 0 \\ \frac{1}{2}\omega_1 & -\frac{1}{2}(J+\delta\omega-\Delta\omega) & 0 & 0 \\ 0 & 0 & \frac{1}{2}(\delta\omega-\Delta\omega) & \frac{1}{2}\omega_1 \\ 0 & 0 & \frac{1}{2}\omega_1 & -\frac{1}{2}(\delta\omega+\Delta\omega) \end{bmatrix} \tag{18}$$

We can examine the other type of ^{13}C "off-resonance" effect by <u>not</u> making the assumption of Equation (10). Therefore, we are saying our ^{13}C radiation is substantial enough to somewhat disturb the other member of the ^{13}C doublet. Thus, it is no longer necessary to assume that $J >> \frac{1}{2}\omega_1$, and we are <u>not</u> so far "off-resonance" from the other ^{13}C transition that it is irrelevant. So proceeding with this in mind, we can use Equation (18) and the Liouville Equation (8) to get the following set of coupled differential equations:

$$\begin{aligned} \dot{\rho}_{13} &= -i\,(\tfrac{1}{2}J + \Delta\omega)\,\rho_{13} + i\,\tfrac{1}{2}\omega_1\,(\rho_{14} - \rho_{23}) \\ \dot{\rho}_{14} &= -i\,(\tfrac{1}{2}J + \Delta\omega + \delta\omega)\rho_{14} + i\,\tfrac{1}{2}\omega_1\,(\rho_{13} - \rho_{24}) \\ \dot{\rho}_{24} &= i\,(\tfrac{1}{2}J - \Delta\omega)\rho_{24} + i\,\tfrac{1}{2}\omega_1\,(\rho_{23} - \rho_{14}) \\ \dot{\rho}_{23} &= i\,(\tfrac{1}{2}J - \Delta\omega + \delta\omega)\rho_{23} + i\,\tfrac{1}{2}\omega_1\,(\rho_{24} - \rho_{13}) \end{aligned} \tag{19}$$

The initial conditions for ρ_{13}, ρ_{14}, ρ_{24}, and ρ_{23} are identical to those in Equations (11). The solution of this set of equations is rather tedious, but the important matrix elements can be shown to be:

$$\rho_{13}(\tau) = \tfrac{1}{2}(A-C)\, e^{-i\Delta\omega\tau} \{i(a \cos \Omega_+\tau + c \cos \Omega_-\tau) + (b \sin \Omega_+\tau + d \sin \Omega_-\tau)\}$$

$$\rho_{24}(\tau) = \tfrac{1}{2}(A-C)\, e^{-i\Delta\omega\tau} \{i(a \cos \Omega_+\tau + c \cos \Omega_-\tau) - (b \sin \Omega_+\tau + d \sin \Omega_-\tau)\} \tag{20}$$

where we have

$$\Omega_\pm = \frac{1}{\sqrt{2}} \{(\tfrac{J}{2})^2 + (\tfrac{J}{2} + \delta\omega)^2 + \omega_1^2 \pm [(\tfrac{J}{2})^4 + (\tfrac{J}{2} + \delta\omega)^4 + \omega_1^4 - 2(\tfrac{J}{2})^2 (\tfrac{J}{2} + \delta\omega)^2 + 2 (\tfrac{J}{2})^2 \omega_1^2 + 2 \omega_1^2 (\tfrac{J}{2} + \delta\omega)^2]^{\frac{1}{2}} \}^{\frac{1}{2}} \tag{21}$$

where Ω_+ refers to the top sign and Ω_- refers to the bottom sign. Also, we have the following values for a, b, c, and d in Equations (20):

$$a = \frac{\Omega_-^2 - (\frac{J}{2})^2}{\Omega_-^2 - \Omega_+^2}$$

$$c = \frac{(\frac{J}{2})^2 - \Omega_+^2}{\Omega_-^2 - \Omega_+^2} \tag{22}$$

$$b = \frac{(\frac{J}{2})[\Omega_-^2 - (\frac{J}{2})^2 - \omega_1^2]}{\Omega_+ (\Omega_-^2 - \Omega_+^2)}$$

$$d = \frac{(\frac{J}{2})[(\frac{J}{2})^2 + \omega_1^2 - \Omega_+^2]}{\Omega_- (\Omega_-^2 - \Omega_+^2)}$$

The following relations also hold true

$$a + c = 1$$

$$\Omega_+ b + \Omega_- d = \frac{J}{2} \tag{23}$$

After the ^{13}C pulse ends, the density matrix evolution is identical to that in Equations(13). Then using Equations (13), (20), and (3) we compute the proton transverse magnetization at $2\Delta T$ to be

$$\langle I_y(2\Delta T)\rangle_{13} = \langle I_y(2\Delta T)\rangle_{24} = \langle I_y(2\Delta T)\rangle_{\tau=0} \{(b \sin \Omega_+\tau + d \sin \Omega_-\tau) + (a \cos \Omega_+\tau + c \cos \Omega_-\tau) \cos (\tfrac{J}{2}\tau)\}$$

$$\langle I_x(2\Delta T)\rangle_{13} = -\langle I_x(2\Delta T)\rangle_{24} = \langle I_y(2\Delta T)\rangle_{\tau=0} \{(b \sin \Omega_+\tau + d \sin \Omega_-\tau) - (a \cos \Omega_+\tau + c \cos \Omega_-\tau) \sin (\tfrac{J}{2}\tau)\} \quad (24)$$

where $\langle I_y(2\Delta T)\rangle_{\tau=0}$ is again the amplitude of either of the peaks of the doublet for the case where $\tau = 0$. Notice that the y-components of the magnetization of the proton doublet are identical, while the x-components merely differ by a sign.

Careful examination of Equations(24) tells us several important things. First of all, we see that neither of the ^{13}C "off-resonance" effects we have considered can possibly lead to the discrepancy in the amplitudes of the peaks in the doublet of the spectra in Figure 3. Any such off-resonance effects may alter the overall amplitudes of the peaks as well as introduce dispersion to the peaks, via the x-components, but the two peaks must remain mirror images of each other in the spectrum. Because of this, we can then rule out magnetic field inhomogeneity as a possible cause of that discrepancy. Magnetic field inhomogeneity can be treated by summing a distribution of peaks being off-resonance by different amounts. However, any distribution of frequency would still lead to overall lineshapes for the two peaks which are mirror images of each other, thus ruling this effect out as a possible

explanation. Also we can precisely determine $\delta\omega$, and consequently, the resonance frequency of the ^{13}C line by observing the effects of dispersion on the lineshape.

The full behavior of the functions in Equation (24) is quite involved. However, we can look at certain limiting cases to separate the two kinds of off-resonance effects. To try to understand the first type of off-resonance effect where the ^{13}C radiation is slight "off" the intended frequency, we can take the limit of Equations(24) in the case where we assume the approximation in Equation (10) to be valid. In this case Equations (24) become:

$$\langle I_y(2\Delta T)\rangle_{13} = \langle I_y(2\Delta T)\rangle_{24} = \langle I_y(2\Delta T)\rangle_{\tau=0} \{\cos\left(\tfrac{1}{2}\sqrt{\omega_1^2 + \delta\omega^2}\,\tau\right)\cos\left(\frac{\delta\omega\tau}{2}\right) + \frac{\delta\omega}{\sqrt{\omega_1^2 + \delta\omega^2}}\sin\left(\tfrac{1}{2}\sqrt{\omega_1^2 + \delta\omega^2}\,\tau\right)\sin\left(\frac{\delta\omega\tau}{2}\right)\}$$

(25)

$$\langle I_x(2\Delta T)\rangle_{13} = -\langle I_x(2\Delta T)\rangle_{24} = \langle I_y(2\Delta T)\rangle_{\tau=0} \{\cos\left(\tfrac{1}{2}\sqrt{\omega_1^2 + \delta\omega^2}\,\tau\right)\sin\left(\frac{\delta\omega\tau}{2}\right) - \frac{\delta\omega}{\sqrt{\omega_1^2 + \delta\omega^2}}\sin\left(\tfrac{1}{2}\sqrt{\omega_1^2 + \delta\omega^2}\,\tau\right)\cos\left(\frac{\delta\omega\tau}{2}\right)\}$$

For the case where $\delta\omega << \omega_1$, we see that Equations (25) are the same as those of Equations (15) except that there is a phase error of $\delta\omega\tau/2$ introduced into the peaks. Thus, both peaks have the same amount of dispersion mixed in, and the sign of that dispersion is opposite for the two peaks. We note that we can use this effect to our advantage in determining the position of the ^{13}C resonances. We could arbitrarily increase τ until any ^{13}C off-resonance, $\delta\omega$, no matter how small, would lead to noticeable phase changes in the proton spectrum;

however, an upper limit on τ, equal to approximately the inverse of the ^{13}C line width, effectively limits the resolution of $\delta\omega$ to the ^{13}C linewidth. Thus, this indirect method of determining the position of the ^{13}C resonance seems to be superior, in this case, to other methods such as spin tickling[6], whose resolution is ultimately limited by the proton rather than the ^{13}C linewidth.

The second type of off-resonance effect, in which we take into account the effect of weakly irradiating the other member of the ^{13}C doublet, can be examined by assuming that

$$\delta\omega = 0 \tag{26}$$

but <u>not</u> making the assumption of Equations(10). Taking the subsequent limiting case of Equations(24) expanded to second order in the parameter $x = \omega_1/J$, we have the following

$$\begin{aligned}
\langle I_y(2\Delta T)\rangle_{13} = \langle I_y(2\Delta T)\rangle_{24} = \langle I_y(2\Delta T)\rangle_{\tau=0} \{ & \cos(\tfrac{1}{2}\omega_1\tau)\,[\cos[(\tfrac{1}{2}\omega_1\tau)(\tfrac{1}{2}x)] \\
& -\tfrac{1}{2}x^2 \sin[(\tfrac{J}{2}\tau)(1+\tfrac{1}{2}x^2)] \sin(\tfrac{J}{2}\tau)\,] \\
& + x \sin(\tfrac{1}{2}\omega_1\tau) \sin[(\tfrac{J}{2}\tau)(1+\tfrac{1}{2}x^2)] \cos(\tfrac{J}{2}\tau)\}
\end{aligned} \tag{27}$$

$$\begin{aligned}
\langle I_x(2\Delta T)\rangle_{13} = -\langle I_x(2\Delta T)\rangle_{24} = \langle I_y(2\Delta T)\rangle_{\tau=0} \{ & \cos(\tfrac{1}{2}\omega_1\tau)\,[\sin[(\tfrac{1}{2}\omega_1\tau)(\tfrac{1}{2}x)] \\
& -\tfrac{1}{2}x^2 \sin[(\tfrac{J}{2}\tau)(1+\tfrac{1}{2}x^2)] \cos(\tfrac{J}{2}\tau)\,] \\
& - x \sin(\tfrac{1}{2}\omega_1\tau) \sin[(\tfrac{J}{2}\tau)(1+\tfrac{1}{2}x^2)] \sin(\tfrac{J}{2}\tau)\}
\end{aligned}$$

Thus, we see for the case of $x \ll 1$ (or $\omega_1 \ll J$) that Equations (27) are the same as Equation (15) except that there is a phase error of $(\omega_1\tau/2)\cdot(x/2)$ introduced into the peaks. Thus, again both peaks have equal and opposite

amounts of dispersion mixed in. If we intend to use the first type of off-resonance effect to find the ^{13}C resonance position by observing the amount of dispersion mixed in, we must take into account also this other phase error due to the second type of off-resonance effect. This does not hurt our resolution of the ^{13}C resonant frequency, but it does mean that we must subtract off this second effect. Although we do not show the results here, computer calculations of Equations (24) indicate that if both types of off-resonance effects are present simultaneously and they are both small, their phase errors will, in fact, merely add linearly rather than combine in some more complicated manner.

Thus, it seems that the detailed spin dynamics of the experiment, taking off-resonance effects into account, seem to provide the necessary insight to use this technique as a very accurate, indirect method of determining the ^{13}C resonant frequency. However, only in the next section, where we investigate the effects of relaxation, can we quantitatively fit the measured peak amplitude to theoretical calculations.

D. Spin Dynamics Including Relaxation Effects but Ignoring Off-Resonance Effects

In order to make the relaxation calculation more tractable and more easily interpretable, we have chosen to ignore both types of ^{13}C off-resonance effects in this section. According to Redfield's theory of relaxation[2], we can include relaxation effects by assuming that we have a modified Liouville equation:

$$\frac{d}{dt}\rho_{mn} = i[\rho, H']_{mn} - \frac{1}{T_{mn}}\rho_{mn} \qquad (m \neq n) \tag{28}$$

Since the relaxation times are long compared to 1/J, we can assume that the damping term in Equation (28) for off-digonal matrix elements depends only

on the same matrix element appearing on the left-hand side of Equation (28). Each different matrix element, ρ_{mn}, however, is assigned its own rate constant, $1/T_{mn}$. This condition of $T_{mn} >> 1/J$ merely means that we do, in fact, have a well-resolved proton doublet to begin with. Furthermore, the requirement is that the real relaxation time $T_{mn} >> 1/J$ and not the apparent $T_{mn}^{*} >> 1/J$ where T_{mn}^{*} is the decay constant taking magnetic field inhomogeneity into account. Thus, this criterion is easily satisfied in our experiment.

Next, by using Equations (28) and also Equations (11), which are the ones appropriate for ignoring off-resonance effects, we can determine the following differential equations:

$$\begin{aligned}
\dot{\rho}_{13} &= -i\,(\tfrac{1}{2}J + \Delta\omega)\rho_{13} + i\,\tfrac{1}{2}\omega_1\,\rho_{14} - \frac{1}{T_{13}}\,\rho_{13} \\
\dot{\rho}_{14} &= -i\,(\tfrac{1}{2}J + \Delta\omega)\rho_{14} + i\,\tfrac{1}{2}\omega_1\,\rho_{13} - \frac{1}{T_{14}}\,\rho_{14} \\
\dot{\rho}_{24} &= \;\;i\,(\tfrac{1}{2}J - \Delta\omega)\rho_{24} + i\,\tfrac{1}{2}\omega_1\,\rho_{23} - \frac{1}{T_{24}}\,\rho_{24} \\
\dot{\rho}_{23} &= \;\;i\,(\tfrac{1}{2}J - \Delta\omega)\rho_{23} + i\,\tfrac{1}{2}\omega_1\,\rho_{24} - \frac{1}{T_{23}}\,\rho_{23}
\end{aligned} \tag{29}$$

Again, the initial conditions are the same as in Equations (11). The relevant matrix elements can then be determined to be

$$\begin{aligned}
\rho_{13}(\tau) = \tfrac{1}{2}i(A-C)\; e^{-i(\frac{1}{2}J+\Delta\omega)\tau}\; e^{-\frac{1}{2}(\frac{1}{T_{13}} + \frac{1}{T_{14}})\tau} \\
\times \left\{\cos\left[\tfrac{1}{2}\sqrt{\omega_1^{\,2} - \left(\frac{1}{T_{13}} - \frac{1}{T_{14}}\right)^2}\;\tau\right] + \frac{\frac{1}{T_{14}} - \frac{1}{T_{13}}}{\sqrt{\omega_1^{\,2} - \left(\frac{1}{T_{13}} - \frac{1}{T_{14}}\right)^2}}\right. \\
\left.\sin\left[\tfrac{1}{2}\sqrt{\omega_1^{\,2} - \left(\frac{1}{T_{13}} - \frac{1}{T_{14}}\right)^2}\;\tau\right]\right\}
\end{aligned} \tag{30}$$

$$\rho_{24}(\tau) = \tfrac{1}{2}i(A-C)\, e^{i(\frac{1}{2}J-\Delta\omega)\tau}\, e^{-\frac{1}{2}(\frac{1}{T_{24}} + \frac{1}{T_{23}})\tau}$$

$$\times \{\cos[\tfrac{1}{2}\sqrt{\omega_1^2 - (\tfrac{1}{T_{24}} - \tfrac{1}{T_{23}})^2}\,\tau] + \frac{(\frac{1}{T_{23}} - \frac{1}{T_{24}})}{\sqrt{\omega_1^2 - (\frac{1}{T_{24}} - \frac{1}{T_{23}})^2}}$$

$$\sin[\tfrac{1}{2}\sqrt{\omega_1^2 - (\tfrac{1}{T_{24}} - \tfrac{1}{T_{23}})^2}\,\tau]\}$$

As in the other cases, the Equations (13) for the evolution of the density matrix after the ^{13}C pulse are still applicable. Then by using Equations (13), (30), and (3), we get

$$\langle I_y(2\Delta T)\rangle_{13} = \langle I_y(2\Delta T)\rangle_{\tau=0}\, e^{-\frac{1}{2}(\frac{1}{T_{14}} - \frac{1}{T_{13}})\tau} \{\cos[\tfrac{1}{2}\sqrt{\omega_1^2 - (\tfrac{1}{T_{14}} - \tfrac{1}{T_{13}})^2}\,\tau]$$

$$+ \frac{(\frac{1}{T_{14}} - \frac{1}{T_{13}})}{\sqrt{\omega_1^2 - (\frac{1}{T_{14}} - \frac{1}{T_{13}})^2}} \sin[\tfrac{1}{2}\sqrt{\omega_1^2 - (\tfrac{1}{T_{14}} - \tfrac{1}{T_{13}})^2}\,\tau]\} \qquad (31)$$

$$\langle I_y(2\Delta T)\rangle_{24} = \langle I_y(2\Delta T)\rangle_{\tau=0}\, e^{-\frac{1}{2}(\frac{1}{T_{23}} - \frac{1}{T_{24}})\tau} \{\cos[\tfrac{1}{2}\sqrt{\omega_1^2 - (\tfrac{1}{T_{23}} - \tfrac{1}{T_{24}})^2}\,\tau]$$

$$+ \frac{(\frac{1}{T_{23}} - \frac{1}{T_{24}})}{\sqrt{\omega_1^2 - (\frac{1}{T_{23}} - \frac{1}{T_{24}})^2}} \sin[\tfrac{1}{2}\sqrt{\omega_1^2 - (\tfrac{1}{T_{23}} - \tfrac{1}{T_{24}})^2}\,\tau]\}$$

$$\langle I_x(2\Delta T)\rangle_{13} = \langle I_x(2\Delta T)\rangle_{24} = 0$$

where we note that $\langle I_y(2\Delta T)\rangle_{\tau=0}$ now implicitly includes an overall relaxation term exp $(-2\Delta T/T_{13})$.

After examination of Equations (31), we see that the effects of the relaxation are three-fold. First, we see that there is an exponential damping or increasing of the amplitude of the peak, depending on the difference of the two relaxation rates. For the case of $\langle I_y(2\Delta T)\rangle_{13}$ we see that the crucial quantity is $(1/T_{14} - 1/T_{13})$. If the two time constants T_{14} and T_{13} are equal, then we see no effects and the magnetization is the same as that in Equation (15). If, however $T_{14} < T_{13}$, then there will be a damping of the amplitude; and if $T_{13} < T_{14}$, then there will be an increase in the peak's amplitude. The second effect of the relaxation is to alter the oscillation frequency; however, this effect is second order in the parameter $R_{13} = (1/T_{14} - 1/T_{13})/\omega_1$. The third effect of the relaxation is to introduce a first order (in R_{13}) term which oscillates like sine rather than cosine. The main effect it has is to uniformly translate the zero-crossings of the amplitudes as it effectively introduces an overall phase error into the oscillating term. This phase of the oscillation is not to be confused with the dispersion-related phase discussed extensively in Section II C of this paper. Although we have not calculated in detail the effects of relaxation and ^{13}C off-resonance effects simultaneously, we feel that we can safely predict the results for small off-resonance parameters by a linear combination of the dispersion phase errors predicted by Equations (25) and (27) and the magnetization predicted by Equations (31).

Fitting the measured amplitude of the peak to the theoretical Equations (31) can yield a value for R_{13}, and knowing ω_1 and T_{13}, this will then yield the relaxation time T_{14}. A similar procedure for the other peak will subsequently yield T_{23} if we know T_{24}. It seems reasonable to assume that

$$T_{13} = T_{24} = (T_2)_I \tag{32}$$

where this just means that the relaxation time constants of the two members of the proton doublet (corresponding to the allowed transitions 1-3 and 2-4) are the same. Furthermore, since these are just the conventional proton T_2's of such a system, we call these times $(T_2)_I$.

In the next section we quantitatively compare theory and experiment and determine values for T_{14} and T_{23}. We also look briefly at some data which show off-resonance effects discussed in Section II C.

III. PRESENTATION AND DISCUSSION OF RESULTS

A. Relaxation Data

In this section we first compare the spin dynamical theory including relaxation, of Section II D, to experimental data. First, we need to rewrite Equations (31) in a slightly more usable form

$$\frac{\langle I_y(2\Delta T)\rangle_{13}}{\langle I_y(2\Delta T)\rangle_{\tau=0}} = e^{-\frac{1}{2}\theta R_{13}} \left\{\cos\left(\tfrac{1}{2}\theta \sqrt{1-R_{13}^2}\right) + \frac{R_{13}}{\sqrt{1-R_{13}^2}} \sin\left(\tfrac{1}{2}\theta \sqrt{1-R_{13}^2}\right)\right\}$$

$$\frac{\langle I_y(2\Delta T)\rangle_{24}}{\langle I_y(2\Delta T)\rangle_{\tau=0}} = e^{-\frac{1}{2}\theta R_{24}} \left\{\cos\left(\tfrac{1}{2}\theta \sqrt{1-R_{24}^2}\right) + \frac{R_{24}}{\sqrt{1-R_{24}^2}} \sin\left(\tfrac{1}{2}\theta \sqrt{1-R_{24}^2}\right)\right\} \tag{33}$$

where we have now normalized the amplitude of each peak to the value for the case of $\tau = 0$. The parameters in Equations (33) have the following values

$$\theta = \omega_1 \tau$$

$$R_{13} = \frac{1}{\omega_1}\left(\frac{1}{T_{14}} - \frac{1}{T_{13}}\right) = \frac{1}{\omega_1}\left(\frac{1}{T_{14}} - \left(\frac{1}{T_2}\right)_I\right) \tag{34}$$

$$R_{24} = \frac{1}{\omega_1}\left(\frac{1}{T_{23}} - \frac{1}{T_{24}}\right) = \frac{1}{\omega_1}\left(\frac{1}{T_{23}} - \left(\frac{1}{T_2}\right)_I\right)$$

The assumption of Equation (32) has been used to justify the substitutions for T_{13} and T_{24} in Equations (34) above.

In Figure 4 we have plotted experimental data and the theoretical Equations (33) for various values of the R parameters. Figure 4A shows the experimentally measured amplitude of the peak of the proton formate doublet which was not attenuated for long values of τ (the right-most member of the doublet in Figure 3). Figure 4B shows the experimental amplitudes of the other peak of the doublet which was strongly attenuated for long values of τ (the left-most member of the doublet in Figure 3). In both Figures 4A and B the ratios of the amplitudes of the doublet peaks to the amplitude for the special case of $\tau = 0$ were plotted in order to facilitate direct comparison with Equations (33). Amplitudes were determined from areas of the experimental peaks, and normalization was accomplished by comparison of the ^1H impurity peak. The triangles indicate data points for experiments where the echo time, $2\Delta T$, was chosen to be 90 msec while the circles indicate data points for experiments where $2\Delta T$ was chosen to be 280 msec. In all experiments, the same value for the strength of the ^{13}C r.f. pulse, ω_1, was used.

The question now arises as to which of the theoretical Equations (33) corresponds to which of the doublet peaks. The ambiguity arises because we do not know the absolute sign of J; hence, we cannot be sure which of the proton transitions, 1-3 or 2-4, is the lower frequency transition. We have the possibilities of irradiating either the high or low frequency member of the ^{13}C doublet, and the system might react with attenuation of either the high or low frequency member of the proton doublet. Analysis reveals that we can unambiguously assign T_{14} and T_{23}, but we cannot determine the sign of J. Let us consider the four cases of irradiating the high ^{13}C (hi_S) or

low ^{13}C (lo_S) transitions, and observing attenuation of the high ^{1}H (hi_I) or low ^{1}H (lo_I) transitions. It turns out that hi_S - hi_I and lo_S - lo_I both predict that $T_{23} < (T_2)_I$, while hi_S - lo_I and lo_S - hi_I predict that $T_{14} < (T_2)_I$. In our case, we experimentally observed only hi_S - hi_I and lo_S - lo_I so we know that $T_{23} < (T_2)_I$.

By the discussion of the preceding paragraph, we now can determine values for R from the data in Figure 4 without worrying about the subscripts on R. Figure 4A has two theoretical curves (Equation (33)) drawn for R = 0 (solid line) and R = 0.02 (dashed line). From these curves we determine that R = .01 ± .01. The value for R and the error limits are somewhat subjectively determined by noting that the curves for R = 0 and for R = .02 seem to nicely bound the scatter in the data. In Figure 4B we have drawn theoretical curves for R = .20 (solid line), R = .18 (dashed line), and R = .22 (dotted line). The curve for R = .20 fits the experimental data best, and the curves for R = .18 and R = .22 bound the scatter in the data rather well. So from this we conclude that R = .20 ± .02 for Figure 4B.

We determined ω_1 from the zero crossing of the experimental data in Figure 4A to be $\omega_1/2\pi$ = 17.9 Hz. This procedure is convenient since, for this unattenuated peak, relaxation effects are small and Equations (33) become equivalent to Equations(15). Another option to determine the value for ω_1 would be to measure the length of a 2π pulse by actually observing the ^{13}C magnetization. By conventional methods we measured $(T_2)_I$ to be 160 msec. Thus, from Figure 4A the value of R = .01 ± .01 means that T_{14} = 140 ± 20 msec. The value of R = .20 ± .02 from Figure 4B means that T_{23} = 35 ± 3 msec. Although not crucial to the experiment, for general information we measured the $(T_2)_S$ (this is the ^{13}C T_2) to be 480 msec, the $(T_1)_I$ (normal proton T_1)

to be 4.2 sec, and $(T_1)_S$ (normal ^{13}C T_1) to be 8.7 sec. All of these times are shorter than would be expected in a system purged of dissolved oxygen.

Using this method, it is now possible to directly measure all of the relaxation rates pertaining to the off-diagonal density matrix elements of such a system. In our case the only four unique non-zero rates have the time constants $(T_2)_I$, $(T_2)_S$, T_{14}, and T_{23}. The full Redfield theory[2] says that the general relaxation of the density matrix is of the form

$$\frac{d}{dt} \rho_{mn} = - \sum_{ij} R_{mnij} \rho_{ij} \tag{35}$$

where the R_{mnij} is a super-matrix. Thus, the relaxation of a particular element of the density matrix in general depends on the values of other elements as well. However, according to our assumption of Equation (28), the relaxation of each off-diagonal element depends only on its own value. This is not the case for diagonal elements even if we still assume that the relaxation times are long compared to 1/J. A recent paper of Mayne, et al.[4] shows a very pretty experiment, performed on the same chemical system we used, which measures all of the elements of the super-relaxation rate matrix, R_{mnij}, which pertain to diagonal elements of the density matrix. So, by performing experiments like these as well as the experiments described here, it is possible to map out the values of the entire 16 x 16 relaxation matrix for this AX system. Generalized versions of this phase interferometric spin spectroscopic technique are easy to generate for more complicated systems such as AX_2, etc.

If the decay times of the peaks had been long compared to the length of our ^{13}C pulse (as might have been the case had we removed dissolved oxygen), there would have been several alternatives. First of all, we could have just increased the time τ until relaxation effects were noticeable. Care should

be used in choosing the proper ω_1 because if during the time τ the value of cos $(\omega_1\tau/2)$ undergoes many cycles, then the inhomogeneity of the ^{13}C r.f. magnetic field (ω_1/γ_S) could cause the proton magnetization to dephase, thus giving rise to an effective decay rate which could interfere with the measurement of the relaxation decay. This will not be a problem if the following criterion is maintained

$$\frac{\Delta\omega_1}{\omega_1} \ll R \tag{36}$$

where R is the dimensionless parameter of Equations(34). The symbol $\Delta\omega_1$ stands for the variation of the ^{13}C r.f. perturbation across the sample, so $\Delta\omega_1/\omega_1$ is the fractional r.f. inhomogeneity, determined by the geometry of the r.f. coil. A second alternative to the initial problem would be to stop the ^{13}C pulse at a time when the proton magnetization has completely disappeared. This would correspond to values of $\theta = \omega_1\tau = \pi, 3\pi, 5\pi$, etc. At that time the state of the system would have ρ_{14} and ρ_{23} as the only non-zero off-diagonal matrix elements, and the system would relax with the corresponding times T_{14} and T_{23}. After waiting some appropriately long time one would "retrieve" the proton magnetization by the application of another selective ^{13}C pulse. Measurement of the magnetization would then yield the desired relaxation times. A method similar to this last suggestion was used in a quadrupolar system by Hatanaka, et al.[5] to measure off-diagonal forbidden transition relaxation rates for spin 5/2 nuclei, ^{27}Al in Al_2O_3. Of these two methods the former should work in all cases, while the later is applicable only when

$$J \gg \left(\frac{1}{T_{ij}} - \left(\frac{1}{T_2}\right)_I \right) \qquad \text{for } i,j = 1,4 \text{ and } 2,3 \tag{37}$$

B. Qualitative Off-Resonance Data

In this section we very briefly present two spectra showing some of the off-resonance effects of the spin dynamics described in Section II, C. Figure 5 contains spectra taken for $\omega_1\tau = 2\pi$ in which the ^{13}C radiation is slightly off-resonance. Both types of off-resonance effects contribute to these spectra. For the value of ω_1 stated earlier, we have the important parameter of Equation (27), $x = .092$. This means that if the ^{13}C offset frequency, $\delta\omega$, is zero, there will be an apparent phase error of about 8^o due to the second type of off-resonance effect. The first kind of off-resonance effect then predicts that irradiating the ^{13}C line at $\delta\omega/2\pi = .8$ Hz should produce spectra with no dispersion present. This can be estimated by setting the apparent phase errors from Equations (25) and (27) equal to each other to get

$$\delta\omega = \frac{\omega_1^2}{2J} \tag{38}$$

Thus, we speak of this ^{13}C irradiation frequency as being the apparent resonance frequency.

Figures 5A and B show spectra taken for the values of the ^{13}C irradiation frequency above and below, respectively, the apparent resonance frequency. These spectra were taken 10 Hz apart, so we would expect to see a phase difference of $\frac{1}{2}\,\delta\omega\tau$ equal to about 101^o. It is difficult to determine from the spectra exactly what the phase errors are because this was not done with a high resolution spectrometer, and thus the dispersion phase signals can overlap somewhat. However, we can still estimate that Figure 5A is about 4 Hz above the apparent resonance frequency and Figure 5B is about 6 Hz below, corresponding to phase errors of $+40^o$ and -60^o. Very accurate measurements could, in principle, be made to very precisely determine the apparent ^{13}C resonance frequency.

IV. IMPLICATIONS OF THE EXPERIMENT

We discuss here two important applications of the experiment described in the foregoing sections. One of these is the precise determination of ^{13}C resonance frequencies through the observation of changes in the ^{1}H spectrum, as described in Section II, C. Since the sensitivity of the technique does not depend on the magnetogyric ratio, γ_S, of the S spins it potentially is a highly desirable method for the detection of low-γ spin resonances. The only condition for being able to perform the experiment is that the doublet of the S-spectrum is well resolved, and under the reasonable assumption that J as well as the linewidth (due to field inhomogeneity) is proportional to γ_S, it is clear that the magnitude of γ_S does not impose any limitation on the applicability of the method. The other main application is the measurement of T_2's associated with forbidden transitions, in our case T_{23} and T_{14}. Although we will not give an extensive treatment of the various relaxation mechanisms that possibly might prevail, we wish to illustrate the particular significance of these relaxation times by the following very simple model. Suppose that the spin relaxation of an AX system is caused by randomly fluctuating local fields ΔH_I and ΔH_S at the sites of the nuclei I and S, respectively, and let us assume that these fields are parallel to the external Zeeman field. Defining $\Delta\omega_I(t) = \gamma_I \Delta H_K(t)$ and $\Delta\omega_S(t) = \gamma_S \Delta H_S(t)$, we then have for the fluctuating random Hamiltonian:

$$H'(t) = \Delta\omega_I(t)\, I_z + \Delta\omega_S(t)\, S_z \qquad (39)$$

Since only diagonal elements are involved in $H'(t)$, the relaxation rates of the various off-diagonal density matrix elements are given by[3]

$$\frac{1}{T_{mn}} = \overline{(H'_n - H'_m)^2}\,\tau \tag{40}$$

where the bar denotes the ensemble average and τ is the correlation time of the fluctuations. Hence, we find for this simple model

$$\begin{aligned}
\left(\frac{1}{T_2}\right)_I &= \frac{1}{T_{13}} = \frac{1}{T_{24}} = \overline{\Delta\omega_I^2}\,\tau \\
\left(\frac{1}{T_2}\right)_S &= \frac{1}{T_{12}} = \frac{1}{T_{34}} = \overline{\Delta\omega_S^2}\,\tau \\
\frac{1}{T_{23}} &= (\overline{\Delta\omega_I^2} + \overline{\Delta\omega_S^2} - \overline{2\Delta\omega_I\Delta\omega_S})\,\tau \\
\frac{1}{T_{14}} &= (\overline{\Delta\omega_I^2} + \overline{\Delta\omega_S^2} + \overline{2\Delta\omega_I\Delta\omega_S})\,\tau
\end{aligned} \tag{41}$$

While the normal relaxation times depend on $\overline{\Delta\omega_I^2}$ and $\overline{\Delta\omega_S^2}$, which measure the strengths of the fluctuating fields, the times T_{23} and T_{14} are in addition related to $\overline{\Delta\omega_I\,\Delta\omega_S}$. Thus, measurement of the T_2's of forbidden transitions provides information about the cross-correlation between the two local fields. One should be aware that this result strongly depends on the particular relaxation mechanism chosen. For instance, fluctuating fields perperdicular to the Zeemen field with very short correlation times give rise to uniform relaxation rates for all the off-diagonal elements of the density matrix,

$$\left(\frac{1}{T_2}\right)_I = \left(\frac{1}{T_2}\right)_S = \frac{1}{T_{23}} = \frac{1}{T_{14}} = \tfrac{1}{2}(\overline{\Delta\omega_I^2} + \overline{\Delta\omega_S^2})\,\tau \tag{42}$$

Nevertheless, we feel that the physical picture emerging from the first example will have general implications, and that knowledge of relaxation times like T_{23} and T_{14} will be of help in the determination of the detailed nature of molecular motions, such as anisotropic tumbling.

Furthermore, the phase interferometric technique is in general applicable whenever we have a system with two or more inequivalent transitions having one quantum mechanical level in common. It can, for instance, be applied to systems consisting of two coupled nuclear spins, a nucleus and a free electron, or a nucleus with quadrupolar interaction.

ACKNOWLEDGMENTS

This effort was supported by the Office of Naval Research. One of us, A. J. Vega, received partial support from NASA (NSG-7275).

+ On leave from the Weizmann Institute of Science, Rehovot, Israel.

REFERENCES

1. M. E. Stoll, A. J. Vega, and R. W. Vaughan, submitted to Physical Review A.
2. A. G. Redfield, IBM J. Res. Develop. 1, 19 (1957); "Advances in Magnetic Resonance"(ed. by J. S. Waugh), Vol. 1, p. 1, Academic Press, New York, 1965.
3. A. Abraham, "Principles of Nuclear Magnetism" Chapter 8, Oxford, Clarendon, 1961.
4. C. L. Mayne, D. W. Alderman, and D. M. Grant, J. Chem. Phys. 63, 2514 (1975).
5. H. Hatanaka, T. Terao, and T. Hashi, J. Phys. Soc. Japan 39, 835 (1975).
6. R. Freeman and W. A. Anderson, J. Chem. Phys. 37, 2053 (1962).

FIGURE CAPTIONS

Figure 1. Energy level diagram for an AX spin system. The α and β represent the two eigenstates spin up and spin down of the spin ½ particle. The first Greek letter represents the state of the ^{1}H spin and the second represents the state of the ^{13}C spin, so that two ^{1}H transitions are shown with single arrows, while the two ^{13}C transitions are shown with double arrows. The numbers 1, 2, 3, 4 are used to refer to the various energy levels or to the eigenstates to which they correspond. The relative Zeeman energies for ^{1}H (56.4 MHz) and ^{13}C (14.2 Mhz) have been drawn to scale, but the effects of the weak coupling have been greatly exaggerated for emphasis.

Figure 2. Radio frequency pulse sequence used. A $\pi/2$ pulse is applied to both ^{1}H transitions. Then a selective pulse of length τ is applied to only one of the ^{13}C transitions. A π pulse is then applied to both ^{1}H transitions at a time ΔT after the $\pi/2$ pulse, which creates a spin echo at a time $2\Delta T$ after the $\pi/2$ pulse. The signal is recored from $2\Delta T(t = 0)$, defined to be the middle of the echo for Fourier transformation.

Figure 3. Proton phase interferometric spectra for different values of τ. The doublet split by 195 Hz is due to the ^{1}H coupled to the ^{13}C in those formate ions containing ^{13}C. The small peak at the center of the doublet is due to the ^{1}H in the formate ions containing spinless ^{12}C, while the large peak on the far left is due to the small amount of ^{1}H impurity in the solvent. The five spectra are for values of τ = 0, 28, 56, 84, and 112 msec, corresponding to values of $\omega_1\tau = 0^{o}$, 180^{o}, 360^{o}, 540^{o}, and 720^{o}.

Figure 4. Comparison of experimental and theoretical values of the amplitudes of the peaks of the proton doublet vs. the value of $\theta = \omega_1\tau$. The amplitudes of the peaks are plotted on the vertical axis, normalized to the peak amplitude for the special case of $\tau = 0$. The value of $\omega_1\tau$ (in degrees) is plotted on the horizontal axis. The triangles indicate experimental data for which the echo time ($2\Delta T$) was 90 msec, and the circles are for $2\Delta T$ = 280 msec. In all cases the same value of ω_1 = 112 rad/sec was used.

A. This solid line corresponds to the theory for the value of the parameter R = 0. The dashed line represents the theory for R = .02.

B. The solid line represents theory for R = .20, the dashed line is R = .18, and the dotted line is R = .22.

Figure 5. Proton phase interferometric spectra (for $\theta = \omega_1\tau = 360^o$) showing ^{13}C off-resonance effects.

A. This spectrum was taken with the ^{13}C irradiation about 4 Hz above the apparent ^{13}C resonance, thus the doublet shows a phase error of about + 40^o.

B. This spectrum was taken with the ^{13}C irradiation about 6 Hz below the apparent ^{13}C resonance, thus the doublet shows a phase error of about - 60^o.

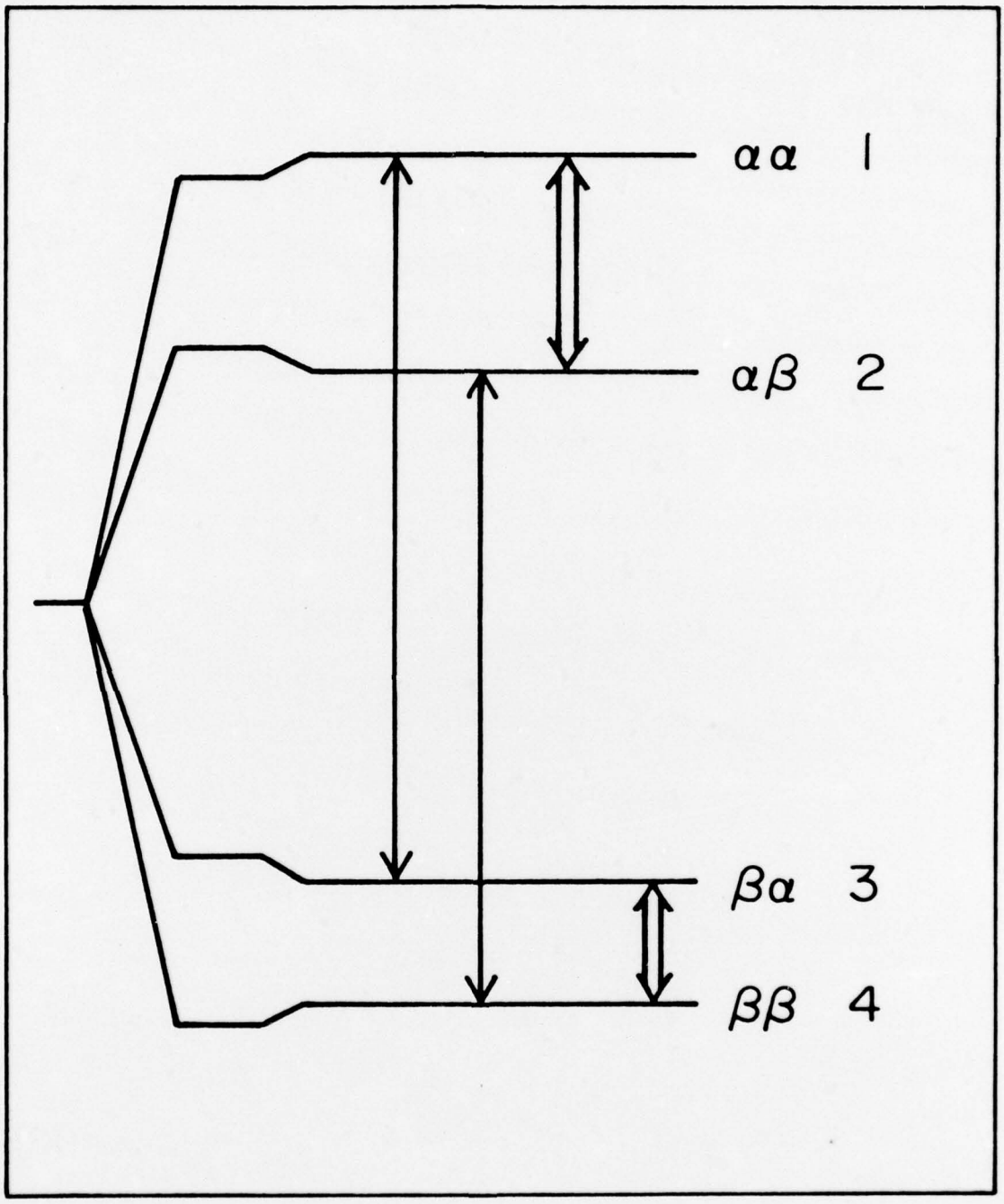

Fig. 1

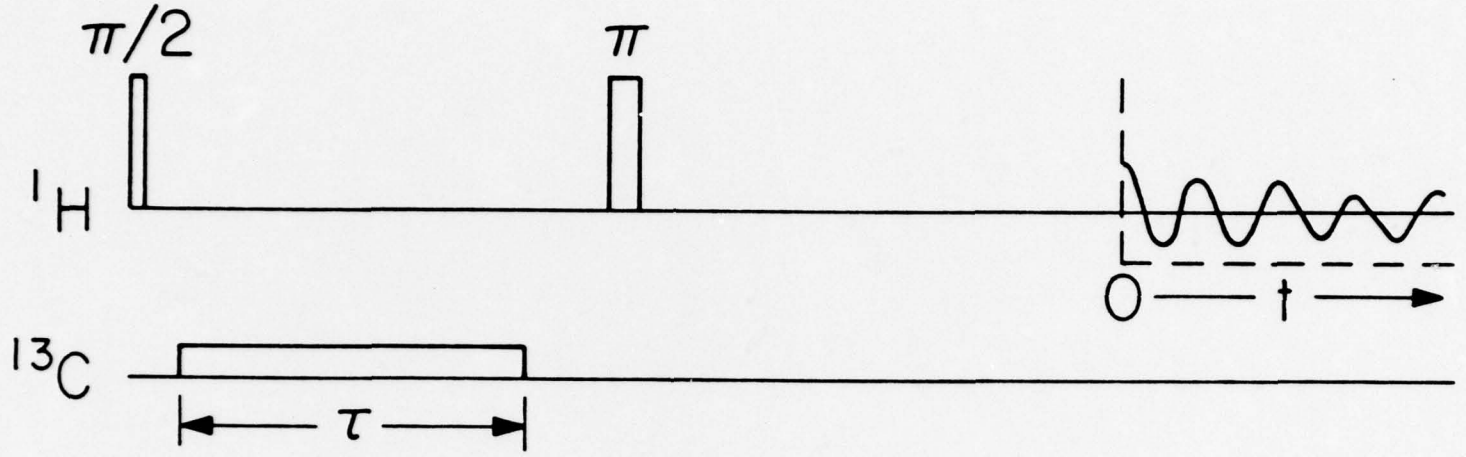

Fig. 2

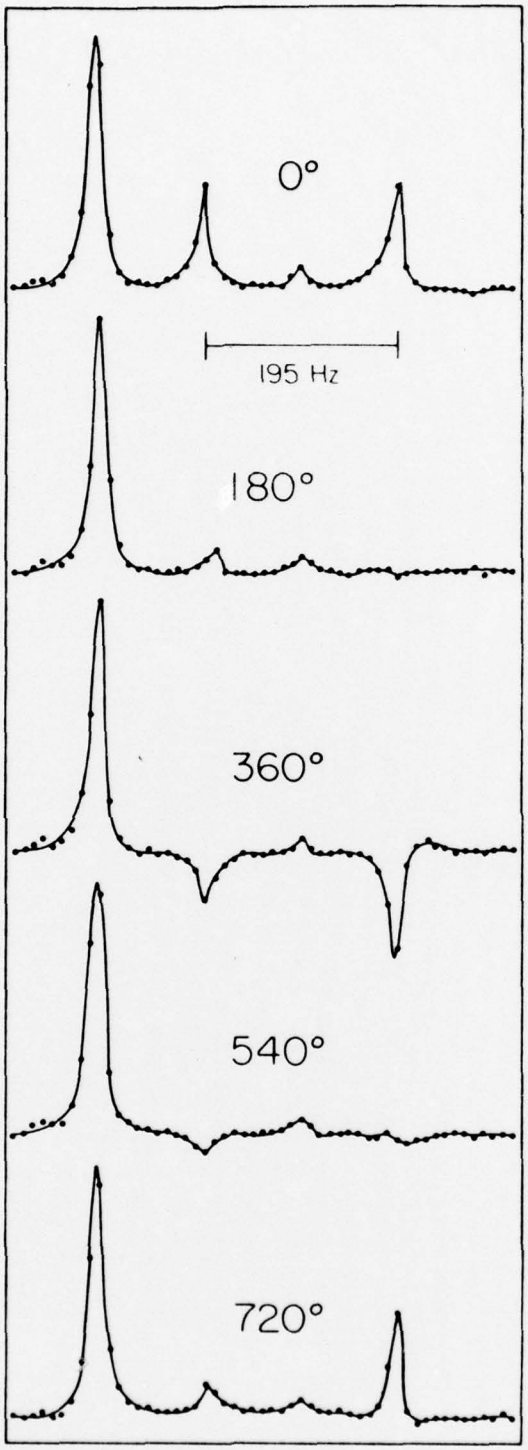

Fig. 3

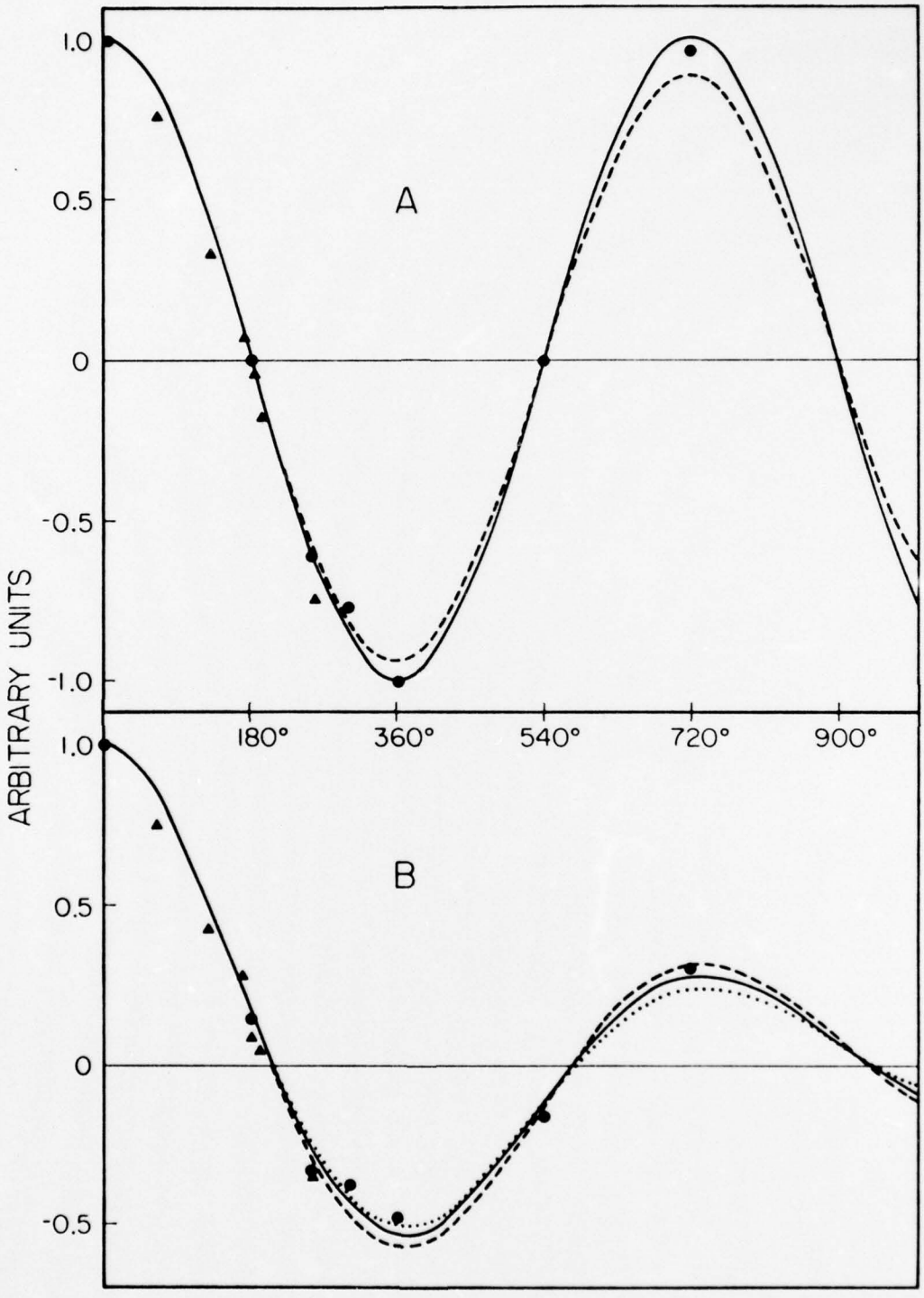

Fig. 4

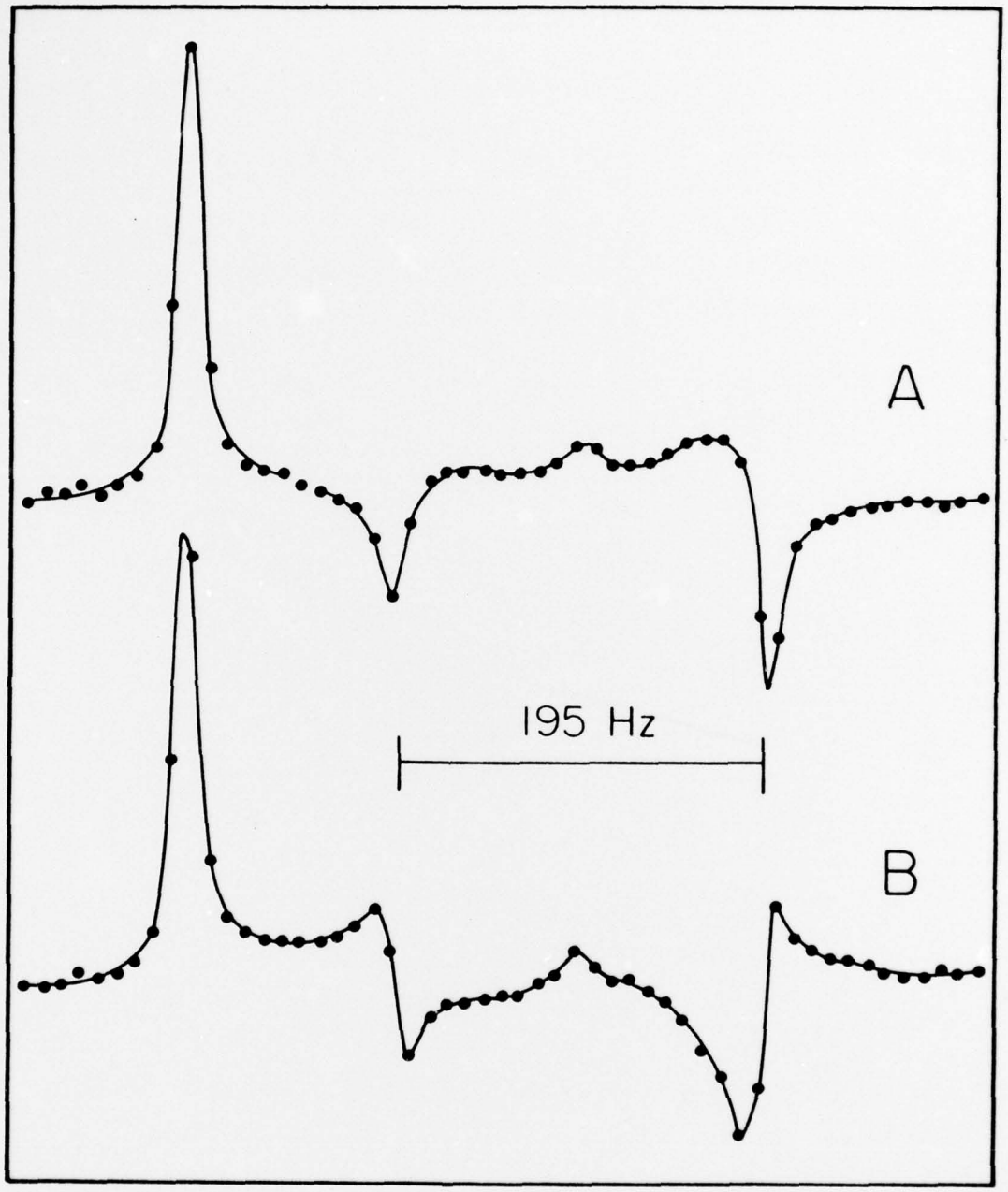

Fig. 5

TECHNICAL REPORT DISTRIBUTION LIST

	No. Copies
Office of Naval Research Arlington, Virginia 22217 Attn: Code 472	2
ONR Branch Office 536 S. Clark Street Chicago, Illinois 60605 Attn: Dr. George Sandoz	1
ONR Branch Office 207 West 24th Street New York, New York 10011 Attn: Scientific Dept.	1
ONR Branch Office 1030 East Green Street Pasadena, California 91106 Attn: Dr. R. J. Marcus	1
ONR Branch Office 760 Market Street, Rm. 447 San Francisco, California 94102 Attn: Dr. P. A. Miller	1
ONR Branch Office 495 Summer Street Boston, Massachusetts 02210 Attn: Dr. L. H. Peebles	1
Director, Naval Research Laboratory Washington, D. C. 20390 Attn: Library, Code 2029 (ONRL) Technical Info. Div. Code 6100, 6170	6 1 1
The Asst. Secretary of the Navy (R&D) Department of the Navy Room 4E736, Pentagon Washington, D. C. 20350	1
Naval Surface Weapons Center White Oak Silver Spring, Maryland 20910 Attn: Code 230	1
Dr. P. R. Antoniewicz University of Texas Department of Physics Austin, Texas 78712	1
Dr. L. N. Jarvis Surface Chemistry Division 5565 Overlook Avenue, S. W. Washington, D. C. 20375	1
Commander, Naval Air Systems Command Department of the Navy Washington, D. C. 20360 Attn: Code 310C (H. Rosenwasser)	1
Defense Documentation Center Building 5, Cameron Station Alexandria, Virginia 22314	12
U. S. Army Research Office P. O. Box 12211 Research Triangle Park, North Carolina 27709 Attn: CRD-AA-IP	1
U. S. Naval Oceanographic Office Library, Code 1640 Suitland, Maryland 20390	1
Naval Ship Research & Development Center Annapolis Division Annapolis, Maryland 21402 Attn: Dr. Allan Evans, Code 2833	1
Commander Naval Undersea Research & Development Center San Diego, California 92132 Attn: Technical Library, Code 133	1
Naval Weapons Center China Lake, California 93555 Attn: Head, Chemistry Division	1
Naval Civil Engineering Laboratory Port Hueneme, California 93041 Attn: Mr. W. S. Haynes	1
Professor O. Heinz Department of Physics & Chemistry Naval Postgraduate School Monterey, California 93940	1
Dr. A. L. Slafkosky Scientific Advisor Commandant of the Marine Corps (Code RD-1) Washington, D. C. 20380	1
Dr. W. M. Risen, Jr. Brown University Department of Chemistry Providence, Rhode Island 02912	1

MAILING LIST

Dr. John B. Hudson
Rennselaer Polytechnic Institute
Materials Engineering Division
Troy, New York 12191

Dr. K. H. Johnson
Massachusetts Institute of Technology
Dept of Metallurgy and Materials Science
Cambridge, Massachusetts 02139

Dr. W. D. McCormick
Dept of Physics
University of Texas
Austin, Texas 78712

Dr. G. A. Somorjai
Dept of Chemistry
University of California/Berkeley
Berkeley, California 94720

Dr. Robert W. Vaughan
California Institute of Technology
Division of Chemistry and Chemical Engineering
Pasadena, California 91125

Dr. David A. Vroom
INTELCOM RAD TECH
P.O. Box 80817
San Diego, California 92138

Dr. J. Bruce Wagner, Jr.
Northwestern University
Evanston, Illinois 60201

Dr. J. M. White
Dept of Chemistry
University of Texas
Austin, Texas 78712

Dr. John T. Yates, Jr.
U.S. Dept of Commerce
National Bureau of Standards
Surface Chemistry Section
Washington, D.C. 20234

Dr. Lennard Wharton
Dept of Chemistry
James Franck Institute
5640 Ellis Avenue
Chicago, Illinois 60637

Dr. J. E. Demuth
International Business Machines Corp.
Thomas J. Watson Research Center
P.O. Box 218
Yorktown Heights, New York 10598

Dr. C. P. Flynn
University of Illinois
Dept of Physics
Urbana, Illinois 61801

Dr. W. Kohn
Department of Physics
University of California (San Diego)
La Jolla, California 92037

Dr. T. E. Madey
National Bureau of Standards
Surface Processes and Catalysis Section
Washington, D.C. 20234

Dr. R. L. Park
Director, Center of Materials Research
University of Maryland
College Park, Maryland 20742

Dr. W. T. Peria
Electrical Engineering Dept
University of Minnesota
Minneapolis, Minnesota 55455

Dr. Narkis Tzoar
City University of New York
Convent Avenue at 138th Street
New York, New York 10031

Dr. R. F. Wallis
Depatment of Physics
University of California/Irvine
Irgine, California 92664

Dr. Chia-wei Woo
Northwestern University
Dept of Physics
Evanston, Illinois 60201

Dr. Mark S. Wrighton
Dept of Chemistry
MIT, Rm 6-335
Cambridge, Massachusetts 02139